

# Who, Where, How Much Is Draining My Battery?

A Multi-factor SOC Prediction Model Based on Thevenin Model

## Summary

Smartphone battery runtime experience is often limited by the inability of existing models to accurately predict remaining usage time under real-world conditions. To address this, we develop a physics-informed model that captures the battery discharge process and provides users with scenario-specific usage guidance, thereby improving both prediction accuracy and practical user experience.

To solve this problem, we construct **an equivalent circuit model** for lithium-ion batteries, enabling continuous-time modeling of state-of-charge (SOC) evolution based on intrinsic electrochemical properties. Assuming an ideal lithium-ion cell, we adopt a **Thevenin circuit** to characterize its electrical behavior. The model drives SOC dynamics through integration of discharge current, describes polarization voltage across the RC branch via a differential equation, and computes terminal voltage using Kirchhoff's laws. This yields a closed-loop system of coupled ordinary differential equations comprising the SOC equation, polarization equation, and current constraint.

Building upon this electrochemical foundation, we further develop a **multi-factor coupled power consumption model** to quantify the contributions of hardware activities and environmental factors under realistic usage. We integrate **internal power modules**, including base, display, CPU/GPU, GPS, and wireless network consumption, onto the battery circuit backbone. Additionally, we introduce **environmental factors** to account for variations in effective capacity and internal resistance due to temperature and cycle aging.

To validate the model, we calibrate parameters and perform numerical simulations using component-level power data from the Google Pixel 8. The coupled differential equations are solved in Python, generating SOC time series under predefined initial states and representative usage scenarios. Based on these simulations, we estimate **time-to-empty time**: for a fully charged Pixel 8, predicted runtimes are approximately 17.1 hours (light usage), 7.7 hours (medium usage), and 4.3 hours (heavy usage).

We further conduct a global sensitivity analysis focusing on the impact of ambient temperature, cycle aging, and base power on SOC prediction. Results show that the model is highly sensitive to temperature and cycle count, but relatively insensitive to variations in base power.

Finally, the model translates into actionable battery management strategies: the operating system should dynamically recalibrate SOC based on real-time load and temperature; applications should suppress unnecessary background activity; and users should avoid high-load operations in low-temperature environments. Moreover, the framework is extensible to electric vehicles by expanding the battery topology and incorporating driving cycles with thermal-electrical coupling, it can enable range prediction, demonstrating its potential across multi-scale energy storage systems.

**Keywords:** State of charge; Thevenin-type Equivalent Circuit Model; Power Consumption Modeling; Dynamic Voltage Response; Time-to-Empty (TTE) Prediction

# Contents

<b>1</b>	<b>Introduction</b>	<b>3</b>
1.1	Problem Background . . . . .	3
1.2	Restatement of Problem . . . . .	3
1.3	Our Work . . . . .	3
<b>2</b>	<b>Assumptions and Justification</b>	<b>4</b>
<b>3</b>	<b>Notation</b>	<b>5</b>
<b>4</b>	<b>Lithium-ion Equivalent Circuit Model</b>	<b>5</b>
4.1	Introduction of Thevenin Equivalent Circuit Model . . . . .	5
4.2	Modeling Process . . . . .	7
4.2.1	SOC Equation . . . . .	7
4.2.2	Polarization Voltage Equation and Terminal Voltage Equation . . . . .	7
4.3	Model Summary and Interpretation . . . . .	8
<b>5</b>	<b>Multi-factor Coupled Power Consumption Model</b>	<b>8</b>
5.1	Additional Contributors . . . . .	9
5.1.1	Base Power Consumption . . . . .	9
5.1.2	Screen Power Consumption . . . . .	9
5.1.3	CPU and GPU Power Consumption . . . . .	9
5.1.4	GPS Power Consumption . . . . .	10
5.1.5	Network Power Consumption . . . . .	10
5.2	Environmental Conditions . . . . .	11
5.2.1	Battery Capacity Loss . . . . .	11
5.2.2	Internal Resistance Variations . . . . .	12
5.3	Optimized Model . . . . .	12
<b>6</b>	<b>Model Validation</b>	<b>12</b>
6.1	Data Preparation . . . . .	13
6.2	Parameter Estimation and Verification . . . . .	13
6.3	Time-to-Empty Predictions . . . . .	17
<b>7</b>	<b>Sensitivity Analysis</b>	<b>19</b>
7.1	Temperature and Cycle Count . . . . .	20
7.2	Baseline Power Consumption . . . . .	21
<b>8</b>	<b>Recommendations</b>	<b>21</b>
8.1	For Users . . . . .	21
8.2	For Manufacturers . . . . .	22
8.3	Model Promotion . . . . .	23
<b>9</b>	<b>Model Evaluation</b>	<b>23</b>
<b>10</b>	<b>Conclusion</b>	<b>24</b>
<b>11</b>	<b>Report on Use of AI Tools</b>	<b>26</b>

# 1 Introduction

## 1.1 Problem Background

In real-world usage, smartphone battery discharge behavior often exhibits significant uncertainty: in some cases, the battery can last an entire day, while in others, the battery level may drop rapidly within a short period of time even without obvious high-intensity usage. This phenomenon not only degrades user experience but also poses challenges for system-level power management and optimization.



Figure 1: Battery management in mobile phones(<https://images.unsplash.com>)

Such behavior is often simply attributed to frequent use or high power consumption of applications, yet it is evident that many other factors are involved. This oversimplified explanation makes it difficult to quantitatively characterize the impact of different usage behaviors on the remaining battery charge and prevents accurate prediction of the remaining operating time under complex usage scenarios.

## 1.2 Restatement of Problem

Based on the background and constraints of the problem, this study investigates the SOC dynamics of lithium-ion batteries in smartphones and addresses the following problems:

- (1) Construct a continuous-time mathematical model using differential equations to describe the smartphone battery's SOC dynamics.
- (2) Extend the model above to incorporate additional contributors such as screen usage, processor load environmental conditions and etc..
- (3) Set different scenarios, substitute real data to predict TTE, and identify the impact of different activities or conditions.
- (4) Conduct sensitivity analysis on the model, identify key influencing factors, and validate the plausibility of the model.
- (5) Provide actionable recommendations for mobile phone suppliers and users on extending phone battery life.

## 1.3 Our Work

In order to avoid complicated descriptions, intuitively reflect our work process, the flowchart is shown in Figure 2:

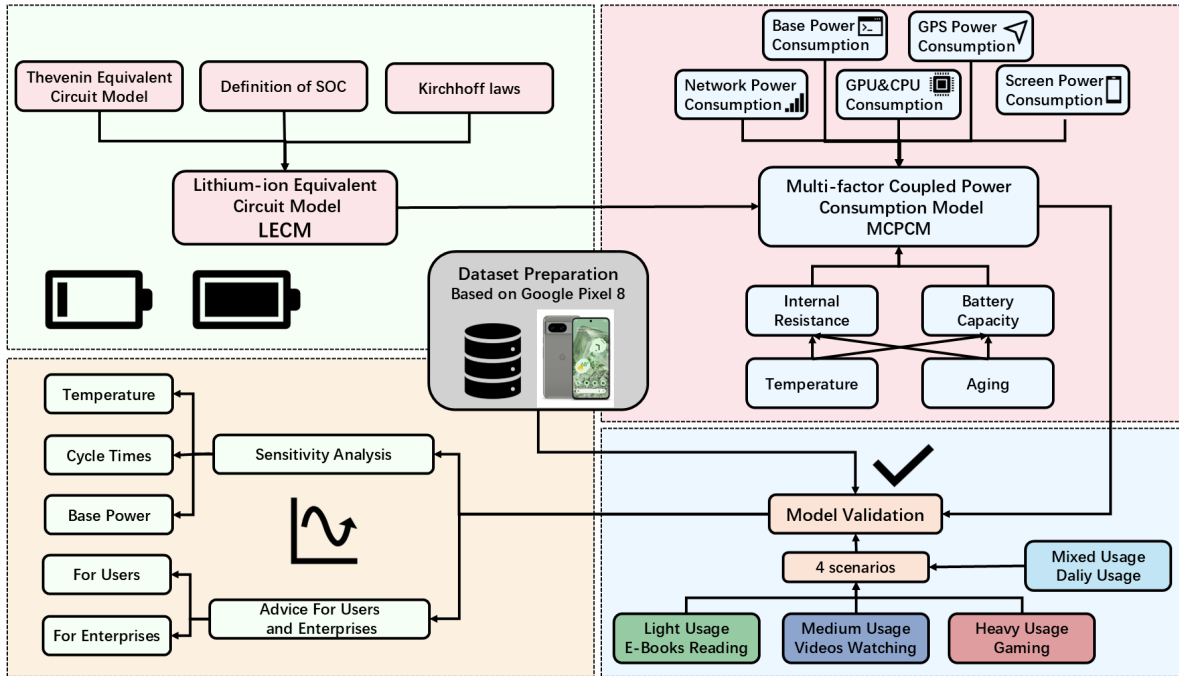


Figure 2: Our work

## 2 Assumptions and Justification

To ensure model tractability while maintaining real-world relevance, the following key assumptions are adopted across our models:

- Battery degradation is modelable and predictable:** The aging behavior of the battery can be accurately described by semi-empirical formulas as functions of observable variables such as cycle count and temperature, enabling these effects to be embedded as dynamic parameters in the discharge simulation.
- Ideal lithium-ion battery assumption:** The model assumes a Coulombic efficiency of 1, meaning all charge inserted into or extracted from the battery is fully reversible, neglecting irreversible losses due to side reactions, self-discharge, etc.
- Electrical behavior can be approximated by an equivalent circuit:** The terminal voltage dynamics are modeled as the sum of the open-circuit voltage, ohmic drop, and polarization voltage from an RC branch; this Thevenin-type equivalent circuit captures key transient phenomena such as voltage hysteresis and recovery with low computational complexity.
- Aging effects manifest primarily as capacity fade and internal resistance increase:** The complex electrochemical degradation mechanisms are simplified into two macroscopic effects: reduced usable capacity and increased internal resistance.
- Certain parameters can be treated as constants:** Physical quantities such as internal resistance and baseline power consumption are assumed constant over relevant time scales, ensuring the tractability and computational efficiency of the differential equation system.

### 3 Notation

The primary notations used in this paper are listed in Table 1.

Table 1: Notation

Symbol	Description	Unit
$SOC(t)$	State of charge	–
$U_{OCV}$	Open-circuit voltage	V
$R_0$	Ohmic internal resistance	$\Omega$
$V(t)$	Terminal voltage	V
$I(t)$	Discharge current	A
$P_{total}(t)$	Time-varying total power	W
$P_i$	Power consumed by a specific component	W
$f$	CPU operating frequency	Hz
$n$	Cycle count	cycles
$T$	Ambient temperature	$^{\circ}\text{C}$
$Q_{loss}$	Capacity loss	Ah
$R_{change}$	Internal resistance increase	$\Omega$

## 4 Lithium-ion Equivalent Circuit Model

In the first step of model construction, we begin by establishing the core differential equation that describes the discharge process of a smartphone battery.

### 4.1 Introduction of Thevenin Equivalent Circuit Model

The state of charge (SOC) is defined as the ratio of the remaining charge  $Q_{\text{res}}$  in a battery to its nominal capacity  $C_n$ , quantifying the proportion of available electrical energy:

$$SOC = \frac{Q_{\text{res}}}{C_n} \quad (1)$$

It is a key metric for battery management and predicting remaining runtime. The change in SOC is directly determined by the battery's discharge current, and its mathematical expression is:

$$SOC(t) = SOC_0(t_0) - \frac{\eta}{C_n} \int_{t_0}^t I(t) dt, \eta = 1 \quad (2)$$

where  $C_n$  is the nominal capacity of the battery,  $I(t)$  is the instantaneous discharge current, and  $\eta$  is the Coulombic efficiency, representing the fraction of charge that can be effectively extracted from the battery. Equation (2) is essentially an application of charge conservation in batteries, describing the dynamic process of the battery's state of charge (SOC) changing over time.

The smartphone is a constant power device, not a constant current device. According to fundamental electrical principles, a battery's discharge process satisfies the basic formula :

$$I(t) = \frac{P_{\text{total}}(t)}{V(t)} \quad (3)$$

where  $P_{total}(t)$  is the total power consumed by the entire phone, while  $V(t)$  and  $I(t)$  represent the battery terminal voltage and discharge current.

A phenomenon often observed by users in actual use: when the battery level is low, the battery seems to deplete significantly faster. As the voltage decreases, the current is forced to increase, thus exacerbating the energy consumption process and creating a discharge behavior similar to an "avalanche effect."

This is because the battery contains complex mechanisms such as resistance, capacitance, and diffusion effects, making the voltage  $V(t)$  and current  $I(t)$  not independent variables; their changes are constrained by the battery's internal electrical characteristics. Therefore, the current  $I(t)$  cannot be directly calculated using only the power relationship.

To address this, we adopt the **Thevenin Equivalent Circuit Model (ECM)**[1], which captures the battery's electrical behavior using simple circuit elementsresistors, capacitors, and a voltage sourcewithout complex electrochemistry. This provides a computable voltage–current relationship to derive  $I(t)$ , effectively modeling transient dynamics under constant-power discharge while retaining physical interpretability. Figure 3 shows the schematic diagram of Thevenin Equivalent Circuit Model.

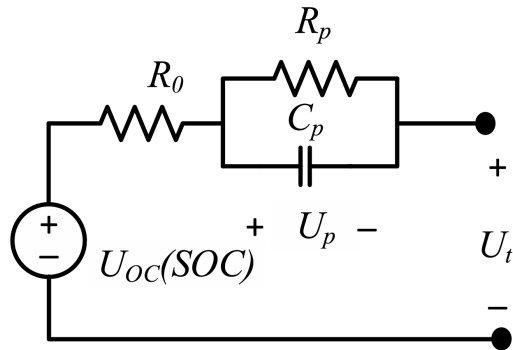


Figure 3: The schematic diagram of Thevenin Equivalent Circuit Model[1]

The model consists of an open-circuit voltage source  $U_{oc}(SOC)$ , an ohmic resistance  $R_0$ , and a parallel polarization branch comprising a polarization resistance  $R_p$  and a polarization capacitance  $C_p$ . The open-circuit voltage varies with the state of charge (SOC),  $R_0$  accounts for instantaneous voltage drop, and the  $R_p-C_p$  branch captures voltage hysteresis and recovery due to polarization effects during charge and discharge.

According to Kirchhoff's law, the terminal voltage is expressed as

$$U_t(t) = U_{OCV}(SOC) - I(t)R_0 - U_p(t) \quad (4)$$

Equation (4) describes the dynamic terminal voltage of a lithium-ion battery. Here,  $U_{OCV}(SOC)$  is the open-circuit voltage, which depends on the state of charge (SOC).  $I(t)R_0$  is the instantaneous ohmic voltage drop across the internal resistance  $R_0$ ; and  $U_p(t)$  is the polarization voltage, capturing dynamic voltage hysteresis due to electrochemical and concentration polarization. Together, these terms determine the ac-

tual output voltage  $U_t(t)$  during discharge and form the core relationship for voltage–current coupling in the equivalent circuit model.

## 4.2 Modeling Process

Building upon the Thevenin equivalent circuit introduced earlier, this subsection constructs a dynamic model based on it, combined with the constant power load assumption, with **SOC**, **polarization voltage**, and **discharge current** as the core variables.

### 4.2.1 SOC Equation

During discharge, charge flows out of the battery through the discharge current  $I(t)$ , causing SOC to decrease over time. From Equation (1) Taking the limit  $\Delta t \rightarrow 0$  gives the continuous-time SOC differential equation:

$$\frac{d \text{SOC}}{dt} = -\frac{I(t)}{C_n}. \quad (5)$$

Equation (5) indicates that the rate of SOC decrease is proportional to the instantaneous discharge current.

### 4.2.2 Polarization Voltage Equation and Terminal Voltage Equation

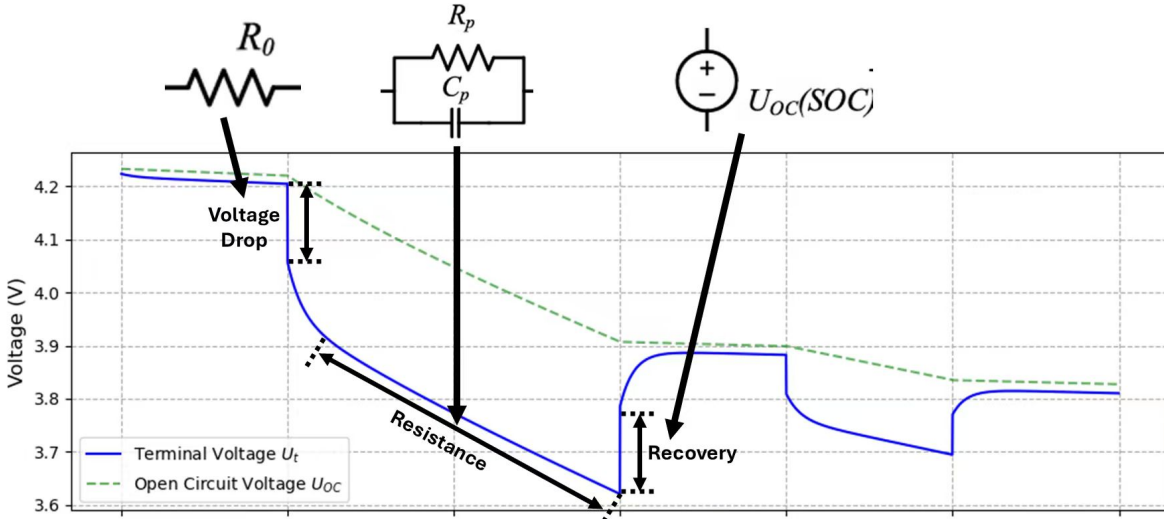


Figure 4: Thevenin Equivalent Circuit Model under data simulation

The dynamics of the polarization voltage  $U_p(t)$  follow Kirchhoff's Current Law (KCL), leading to the differential equation:

$$C_p \frac{dU_p}{dt} = I(t) - \frac{U_p}{R_p}. \quad (6)$$

Equation (6) reveals that the polarization voltage changes are driven by two factors: the input current  $I(t)$ , and the resistive discharge through  $R_p$ . It captures the transient response of the battery to load changes and gradually adjusts.

Rewriting the above equation in standard linear form yields the commonly used *Polarization Voltage Equation*:

$$\frac{dU_p}{dt} = -\frac{1}{R_p C_p} U_p + \frac{1}{C_p} I(t), \quad (7)$$

where the term  $-\frac{1}{R_p C_p} U_p$  represents the natural decay of the polarization voltage, and  $\frac{1}{C_p} I(t)$  represents the increment caused by the input current. Under a constant power load  $P(t)$ , the relationship between terminal voltage and current can be expressed as:

$$P(t) = U_t(t) \cdot I(t) = [U_{OCV}(\text{SOC}) - U_p(t) - I(t)R_0] \cdot I(t), \quad (8)$$

This reflects the nonlinear coupling between battery output current and internal voltage states under constant power conditions.

Solving this quadratic equation for the instantaneous discharge current yields:

$$I(t) = \frac{U_{OCV}(\text{SOC}) - U_p(t) - \sqrt{[U_{OCV}(\text{SOC}) - U_p(t)]^2 - 4R_0 P(t)}}{2R_0}. \quad (9)$$

This solution provides the actual discharge current based on the battery state and load conditions. Combined with the polarization voltage equation, it allows dynamic computation of the terminal voltage  $U_t(t)$ , forming a unified framework that links SOC, polarization voltage, and discharge current.

### 4.3 Model Summary and Interpretation

Ultimately, we obtain a set of coupled equations that fully describe the battery's dynamic behavior.

$$\begin{cases} \frac{d\text{SOC}}{dt} = -\frac{I(t)}{Q_{\text{total}}} \\ \frac{dU_p}{dt} = \frac{I(t)}{C_p} - \frac{U_p}{R_p C_p} \\ I(t) = \frac{(U_{OC} - U_p) - \sqrt{(U_{OC} - U_p)^2 - 4R_0 P_{\text{load}}}}{2R_0} \end{cases} \quad (10)$$

While the model effectively captures the key dynamics of battery discharge, it does not account for other internal or external latent factors, such as temperature variations, aging effects, or complex electrochemical interactions. These simplifications may limit its accuracy under certain operating conditions. To address these limitations and improve predictive performance, the next section focuses on model optimization and refinement strategies.

## 5 Multi-factor Coupled Power Consumption Model

In this section, we refine the model by incorporating multiple factors to improve its predictive accuracy and better capture the battery's dynamic behavior under real-world operating conditions.

## 5.1 Additional Contributors

To more accurately describe the energy consumption process of the battery, the total power  $P_{\text{total}}(t)$  can be expressed as the sum of several components, as shown below:

$$P_{\text{total}}(t) = P_{\text{base}} + P_{\text{screen}}(t) + P_{\text{CPU}}(t) + P_{\text{GPU}}(t) + P_{\text{GPS}} + P_{\text{network}}(t) + \dots \quad (11)$$

By treating these components as independent sub-models, we can analyze and optimize the power consumption of each factor separately.

### 5.1.1 Base Power Consumption

Base power consumption is the constant power[2] drawn by the device in an idle state, arising from background tasks such as app updates, data synchronization and notification checks, the baseband maintaining network connectivity through periodic signal probing, and low-power hardware components such as sensors, real-time clocks, and system monitoring modules. Although the power consumed by each component is small, their cumulative effect over extended idle periods can significantly impact battery life.

It is typically set as a constant. The exact value can be adjusted based on factors like the number of background tasks, network signal strength, and communication frequency.

### 5.1.2 Screen Power Consumption

The power consumption of OLED screens is closely related to the content displayed and the brightness of the screen[2][3]. According to the study by M. Dong and L. Zhong in their paper "Chameleon: A Color-Adaptive Web Browser for Mobile OLED Displays," the power consumption of OLED screens varies significantly depending on the displayed color. The model assumes that the power consumption of the OLED screen is not only dependent on the screen's on/off state but also on the type and brightness of the displayed content. Thus, the screen power consumption  $P_{\text{screen}}(t)$  is expressed by the following formula:

$$P_{\text{screen}}(t) = B(t) \cdot (k_r R + k_g G + k_b B) \quad (12)$$

where  $B(t) \in [0, 100\%]$  denotes the screen brightness at time  $t$ . The color channels  $R, G, B \in [0, 255]$  represent the red, green, and blue components of the displayed content, and the coefficients  $k_r, k_g, k_b$  quantify the energy contribution of each color channel to the total screen power.

### 5.1.3 CPU and GPU Power Consumption

The modeling process for GPUs and CPUs is basically the same.

According to CMOS circuit principles, since power is proportional to the square of the voltage and to the frequency[4], the power consumption of the CPU and GPU, denoted as  $P_{\text{CPU}}$  and  $P_{\text{GPU}}$ , is primarily dominated by dynamic power and can be expressed as

$$P = C \cdot V^2 \cdot f \quad (13)$$

where  $C$  is the equivalent switched capacitance,  $V$  is the supply voltage, and  $f$  is the clock frequency. Moreover,  $V$  and  $f$  are positively correlated; higher frequencies typically require higher operating voltages to ensure circuit stability.

#### 5.1.4 GPS Power Consumption

The power consumption of the GPS module primarily depends on its operating mode, which can be classified as either “Active” or “Sleep”[2]. In the Active mode, the GPS continuously receives satellite signals and computes location, resulting in higher power consumption. In Sleep mode, the module performs minimal operations, which consumes significantly less power. Factors such as the number of visible satellites, signal strength, and environmental conditions may influence power consumption, their impact on system-level power modeling is relatively small and can be considered negligible. Based on this simplification, the GPS power consumption can be expressed as:

$$P_{\text{GPS}} = P_1 \cdot \delta(t) + P_{\text{sleep}} \quad (14)$$

where  $P_1$  represents the power consumed in Active mode,  $\delta(t)$  is an indicator function that equals 1 when the GPS is active and 0 otherwise, and  $P_{\text{sleep}}$  denotes the power consumed in Sleep mode.

#### 5.1.5 Network Power Consumption

The total network power consumption is decomposed into Wi-Fi and Bluetooth power, and cellular network power[2], expressed as

$$P_{\text{network}}(t) = P_{\text{WLANBT}}(t) + P_{\text{ce}}(t). \quad (15)$$

Here,  $P_{\text{WLANBT}}(t)$  represents the power consumption of short-range wireless interfaces such as Wi-Fi and Bluetooth. In contrast,  $P_{\text{ce}}(t)$  denotes the power consumption of cellular communication, which involves long-range transmission to base stations, strongly influenced by network state, signal quality, and data activity.

#### WLAN and Bluetooth

A piecewise linear model for Wi-Fi power consumption, defined by the following equation:

$$P_{\text{WiFi}}(t) = \begin{cases} P_{\text{base}}, & \text{if } D(t) < D_{\text{thresh}} \\ P_{\text{active\_base}} + E_{\text{byte}} \cdot D(t), & \text{if } D(t) \geq D_{\text{thresh}} \end{cases} \quad (16)$$

When the data rate is below the threshold, the Wi-Fi module remains in an idle state with constant power consumption  $P_{\text{base}}$ . When the rate exceeds the threshold, the module switches to active transmission mode, and its power consumption consists of a fixed baseline  $P_{\text{active\_base}}$  plus a dynamic component proportional to the data rate, scaled by the per-unit-data energy cost  $E_{\text{byte}}$ .

#### Cellular Networks

The power consumption of the cellular network module primarily depends on its communication state, and the power difference between states can be significant. In the IDLE state, the module only receives paging signals, maintaining minimal power consumption. In the CELL\_FACH state, the module uses a shared forward access channel for low-speed data transmission, resulting in medium power consumption.

In the CELL\_DCH state, the module transmits large volumes of data via a dedicated high-speed channel, which corresponds to the highest power consumption.

To incorporate these variations into the model, the cellular network power can be expressed in a state-driven form:

$$P_{ce} = \begin{cases} P_{idle}, & \text{state} = \text{IDLE} \\ P_{FACH}, & \text{state} = \text{FACH} \\ P_{DCH}, & \text{state} = \text{DCH} \end{cases} \quad (17)$$

This equation indicates that the network power dynamically depends on the module's state, allowing the model to select the corresponding power consumption in real time.

## 5.2 Environmental Conditions

Although the previously established model can simulate battery power consumption under internal loads, the battery's behavior in real-world usage is often more complex. Temperature significantly affects chemical reaction rates and internal resistance. Over time, the battery also undergoes cycle aging, reducing capacity and altering terminal voltage and internal resistance characteristics. In addition, the internal resistance itself is not constant, but dynamically changes with temperature, aging, and load conditions, further affecting instantaneous current distribution and power consumption.

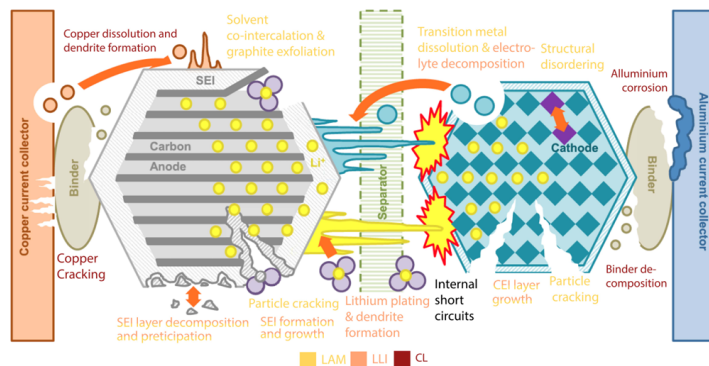


Figure 5: Aging Mechanisms in LIBs[5]

### 5.2.1 Battery Capacity Loss

We adopt a semi-empirical degradation formula as the modeling foundation, expressed in its general form as

$$Q = D e^{F + \frac{G}{T+H}} n^E + n^I + J[5][6] \quad (18)$$

The exponential term  $e^{F + \frac{G}{T+H}}$  captures the temperature dependence of capacity fade, similar to an Arrhenius relationship, reflecting that high temperatures accelerate chemical reactions and capacity loss, while low temperatures slow down the degradation process. The power term  $n^E$  represents the nonlinear cumulative effect of cycle number, describing how capacity gradually decreases with repeated charge-discharge

cycles. The additional term  $n^I + J$  accounts for small deviations in early cycles or low-cycle regions, improving the fit to experimental observations.

### 5.2.2 Internal Resistance Variations

We adopt a semi-empirical formula expressing the internal resistance  $R$  as a function of temperature  $T$  and cycle number  $n$ :

$$R = S e^{\frac{U}{T+V}} e^{\frac{W}{n+Z}} + Z[6] \quad (19)$$

In this equation, the first exponential term  $e^{\frac{U}{T+V}}$  captures the modulation of temperature on internal resistance, the second exponential term  $e^{\frac{W}{n+Z}}$  reflects the cumulative effect of cycle aging, and the constant  $Z$  represents the baseline resistance of the battery.

## 5.3 Optimized Model

Based on the previous subsystem power modeling, we unify the main dynamics of the battery discharge process into a single computational framework, resulting in the following final model:

$$\begin{cases} \frac{dSOC}{dt} = -\frac{I(t)}{Q_{rated} - Q_{loss}} \\ \frac{dU_p}{dt} = \frac{I(t)}{C_p} - \frac{U_p}{R_p C_p} \\ I(t) = \frac{(U_{OC} - U_p) - \sqrt{(U_{OC} - U_p)^2 - 4R_{change}P_{total}}}{2R_{change}} \\ P_{total}(t) = P_{base} + P_{screen}(t) + P_{CPU}(t) + P_{GPU}(t) + P_{GPS} + P_{network}(t) + \dots \end{cases} \quad (20)$$

This model consists of four coupled equations that describe the key dynamics of battery discharge.

The model consists of three coupled equations that capture key battery dynamics under real-world usage. The first describes SOC evolution, where the rate of change depends on instantaneous current  $I(t)$  and the effective capacity  $Q_{rated} - Q_{loss}$ , with  $Q_{loss}$  accounting for capacity fade due to temperature, aging, and resistance effects. The second models the polarization voltage  $U_p$  via an RC branch ( $R_p, C_p$ ), representing the delayed voltage response to load changes. The third computes  $I(t)$  from the terminal voltage, open-circuit voltage  $U_{OC}$ , and total power demand  $P_{total}(t)$ , incorporating a dynamic internal resistance  $R_{change}$  that reflects aging and thermal conditions. Finally,  $P_{total}(t)$  is decomposed into major subsystemsbase, screen, CPU, Wi-Fi, GPS, and cellularenabling detailed power analysis while allowing flexibility for unmodeled loads.

Overall, the model improves the accuracy of terminal voltage and system-level power predictions. Therefore, the next section focuses on model validation, comparing model predictions of terminal voltage, SOC, and current with experimental measurements to evaluate accuracy and provide a foundation for further refinement.

## 6 Model Validation

To evaluate the effectiveness of the proposed battery and system-level power consumption model, this section focuses on parameter calculation and model validation using measured data.

## 6.1 Data Preparation

This work[7] presents an experimental analysis of power consumption on smartphones under various application workloads and system operating conditions, providing a reliable data foundation for smartphone power and battery modeling.

Device parameters are shown in Table 2:

Table 2: Experimental Device Specifications

Parameter	Value
Device Model	Google Pixel 8
Operating System	Android 15
Battery Capacity	4575 mAh
Battery Voltage	4.4 V
Chip	Google Tensor G3
CPU Configuration	$1 \times 2.91 \text{ GHz} (\text{prime}) + 4 \times 2.4 \text{ GHz} (\text{mid}) + 4 \times 1.7 \text{ GHz} (\text{little})$

The resulting dataset captures realistic power consumption characteristics of a commercial smartphone, reflecting the combined effects of application workloads and system-level operations. In this work, the reported experimental measurements are adopted as ground-truth data for parameter fitting and model validation, enabling an objective evaluation of the proposed model's accuracy in predicting current, terminal voltage, and overall power consumption.

## 6.2 Parameter Estimation and Verification

### Some constants( $P_{base}$ , $P_{GPS}$ )

In our idealized model, the base power consumption is set to a constant 200 mW[8], representing the minimum power required to maintain essential smartphone functions during standby, such as background tasks, system clock operation, and basic connectivity.

Similarly, GPS power consumption is modeled as a constant value, as its RF and processing units typically operate at a relatively stable power level once active especially under good signal conditions. While this simplification ignores minor fluctuations, it enables efficient system-level power decomposition and rapid battery runtime estimation.

### Screen Power Consumption ( $P_{\text{screen}}(t)$ )

Based on empirical measurements, the screen power consumption is modeled as:

$$P_{\text{screen}} = B(t) \cdot (4.17 R + 8.81 G + 20.82 B) + 78482, \quad (21)$$

where power is expressed in microwatts ( $\mu\text{W}$ ),  $R, G, B \in [0, 255]$  denote the red, green, and blue pixel intensities of the displayed content, and  $B(t) \in [0, 1]$  represents normalized screen brightness. The model achieves a coefficient of determination  $R^2 = 0.846$ , indicating that approximately 84.6% of the variance in screen power is captured by the formulation.

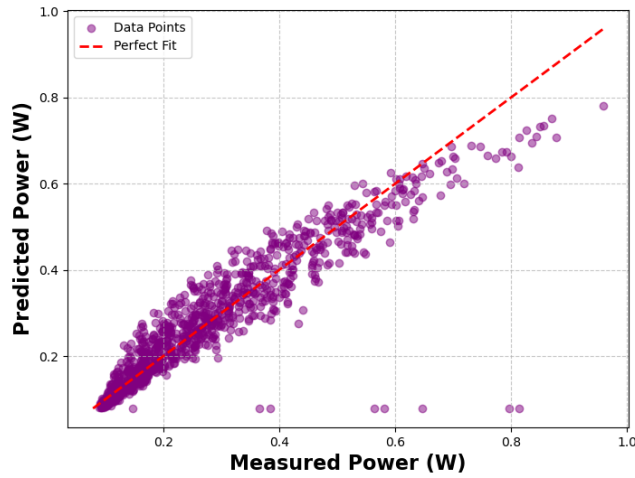


Figure 6: Screen Power Modeling

This result is further corroborated by the scatter plot of predicted versus measured power (Figure 6), which shows that the majority of data points cluster closely around the ideal diagonal line (perfect fit).

#### CPU and GPU Power Consumption ( $P_{\text{CPU}}(t), P_{\text{GPU}}(t)$ )

Although the voltage  $V$  is positively correlated with frequency  $f$ , there exists a minimum startup voltage  $V_{\min}$  below which the processor cannot operate. Hence, the voltage-frequency relationship can be approximated as  $V(f) = V_{\min} + \alpha f$ .

Substituting the voltage-frequency relationship into the dynamic power formula yields a frequency-driven power expression:

$$P(f) \propto f \cdot (V_{\min} + \alpha f)^2 = f \cdot (V_{\min}^2 + 2\alpha V_{\min} f + \alpha^2 f^2) \quad (22)$$

Due to the existence of startup voltage and the nonlinear voltage-frequency relationship, directly using  $V^2 f$  cannot accurately predict processor power across all frequencies. Therefore, a cubic polynomial (third-order) fit is adopted:

$$P(f) = c_0 + c_1 f + c_2 f^2 + c_3 f^3 \quad (23)$$

where  $c_0$  represents static power, and  $c_1$ ,  $c_2$ , and  $c_3$  correspond to the low-frequency startup voltage-dominated term, the cross-term, and the ideal DVS dynamic term, respectively. The cubic polynomial fitting approach allows the model to account for startup voltage constraints, nonlinear frequency scaling, and DVS dynamic effects simultaneously.

To describe the utilization of heterogeneous computing resources, both CPU and GPU operational data are considered. The CPU consists of large, medium, and small cores, and the usage data are classified into light, moderate, and heavy levels. CPU data are grouped according to core types, while GPU data reflect utilization under different workloads. These data are used for model construction and parameter estimation.

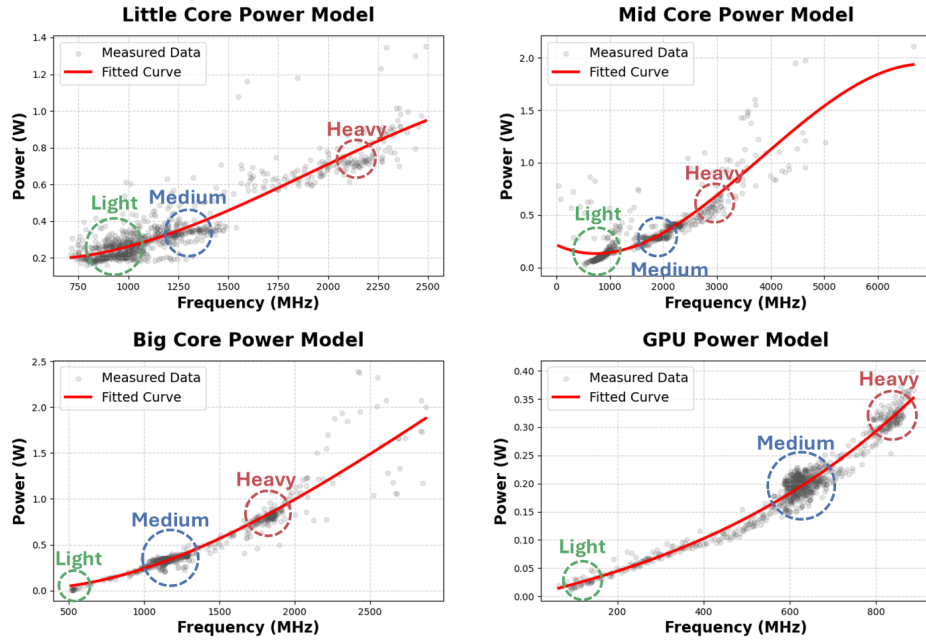


Figure 7: CPU/GPU Power Modeling

Table 3: Power Modeling Results for Compute Components

Component	Static Power (W)	$c_1$	$c_2$	$c_3$	$R^2$
Little Core	0.3108	$-4.78 \times 10^{-4}$	$5.20 \times 10^{-7}$	$-9.03 \times 10^{-11}$	0.8607
Mid Core	0.2167	$-2.37 \times 10^{-4}$	$1.79 \times 10^{-7}$	$-1.57 \times 10^{-11}$	0.8013
Big Core	0.0238	$-1.42 \times 10^{-4}$	$4.03 \times 10^{-7}$	$-4.44 \times 10^{-11}$	0.9045
GPU	0.0016	$1.91 \times 10^{-4}$	$8.99 \times 10^{-8}$	$1.59 \times 10^{-10}$	0.9586

The power modeling results based on a third-order polynomial fit reveal distinct characteristics across compute components (Figure 6 & Table 3). Following the third-order polynomial power modeling, k-means clustering was applied to the power-frequency data of each component. The analysis consistently revealed three distinct and well-separated clusters across all core types (little, mid, and big) as well as the GPU, corresponding to low-, medium-, and high-intensity workload regimes. This trimodal pattern indicates that power consumption is significantly influenced by runtime workload intensity beyond what frequency alone can capture. These findings underscore the importance of incorporating real-time workload classification into fine-grained power management strategies, such as dynamic voltage and frequency scaling (DVFS) or energy-aware scheduling, to improve the accuracy of power prediction and control.

### Network Power Consumption

Analysis of combined Wi-Fi and Bluetooth power consumption reveals a weak correlation with data throughput, yielding a low coefficient of determination ( $R^2 = 0.42$ ). This indicates that transmitted bytes account for only a small fraction of total energy use. Instead, the majority of power typically 150-250 mW even at near-zero throughput is consumed by protocol overhead (Figure 8). This observation reinforces that wire-

less energy efficiency is limited not by data transmission (with  $E_{\text{byte}} \approx 6.2 \text{ nJ/Byte}$ ) but by persistent radio activity during standby ( $P_{\text{base}} \approx 196 \text{ mW}$ ). And the final formulation can be expressed as:

$$P_{\text{WLANBT}} = 196mW + 6.2nJ/\text{Byte} \cdot D(t) \quad (24)$$

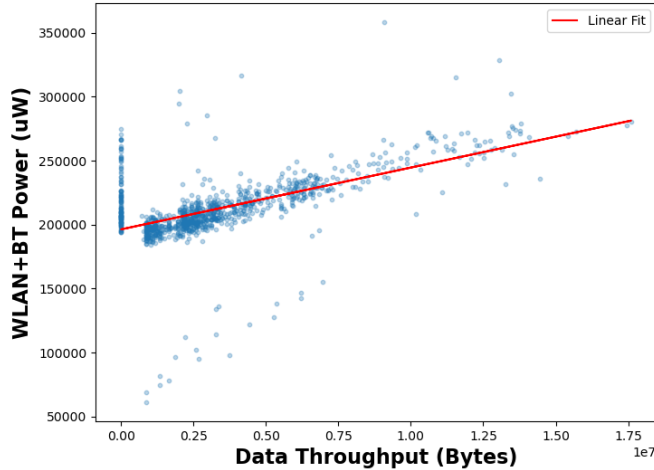


Figure 8: Network Power Modeling

The cellular radio exhibits remarkably stable power consumption, with a mean of  $5.7540 \text{ mW}$  and a low variance of  $\sigma^2 = 1.3827 \text{ mW}^2$  across 1000 samples. As shown in Figure 9, over 95% measurements lie within the concentration interval of  $4.57$  to  $6.90 \text{ mW}$ . Unlike Wi-Fi or Bluetooth, whose power scales (albeit weakly) with throughput, cellular power remains largely decoupled from user data volume under typical conditions. This near-constant behavior justifies modeling it as a fixed baseline component ( $P_{\text{cellular}} \approx 5.75 \text{ mW}$ ) in system-level energy accounting.

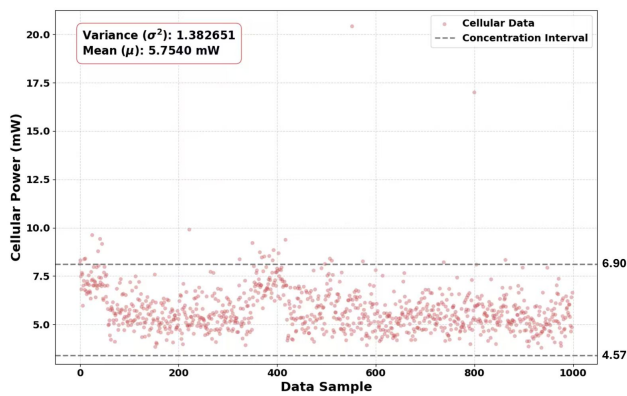


Figure 9: Cellular Power Modeling

### Temperature Effects and Aging Effects

Based on experimental data and fitting results reported in the literature, the numerical form of the formula can be expressed as:

$$Q_{\text{loss}} = 0.0119 e^{-27.78 + \frac{432}{T+20.38}} n^{3.968} + n^{0.4305} - 1.576[6] \quad (25)$$

This expression quantitatively captures the combined effects of temperature and cycle number on capacity degradation. Specifically, the exponential term  $e^{-27.78 + \frac{432}{T+20.38}}$  represents the temperature effect, with high temperatures accelerating capacity loss and low temperatures slowing it down; the power term  $n^{3.968}$  describes the cumulative effect of cycling, reflecting the nonlinear decline of capacity; and the additional term  $n^{0.4305} - 1.576$  captures early-cycle or small deviations. Incorporating this fitted model into the battery simulation allows dynamic adjustment of SOC calculations under varying temperature and cycling conditions, while mapping capacity fade to terminal voltage and internal resistance predictions. The model thus achieves accurate simulation of battery performance under realistic operating conditions, preserving physical interpretability and ensuring high fidelity to experimental data, providing a reliable foundation for system-level power analysis and battery management strategies.

Based on experimental fitting reported in the literature, the numerical expression for our battery is:

$$R_{\text{change}} = 93.5 e^{\frac{-16.13}{T-1.5}} e^{\frac{-915}{n+35.38}} + 35.38[6] \quad (26)$$

This formula captures how internal resistance evolves with temperature and cycle number, and provides a basis for dynamically adjusting the polarization voltage and terminal voltage in the model. Conceptually, as the battery “ages” and environmental conditions change, its increasing internal resistance signals that current flow becomes more difficult, affecting both terminal voltage and SOC dynamics. To account for these effects, the combined impact of internal resistance variations is incorporated into the SOC correction factor  $\eta$ , ensuring that SOC and terminal voltage predictions remain reliable across different temperatures and cycle states.

### 6.3 Time-to-Empty Predictions

We categorize smartphone usage into three intensity levels: light, medium, and heavy, with specific representative activities listed in the figure. Based on this classification, we simulate the evolution of state of charge (SOC) over time under different usage scenarios(Figure 10).

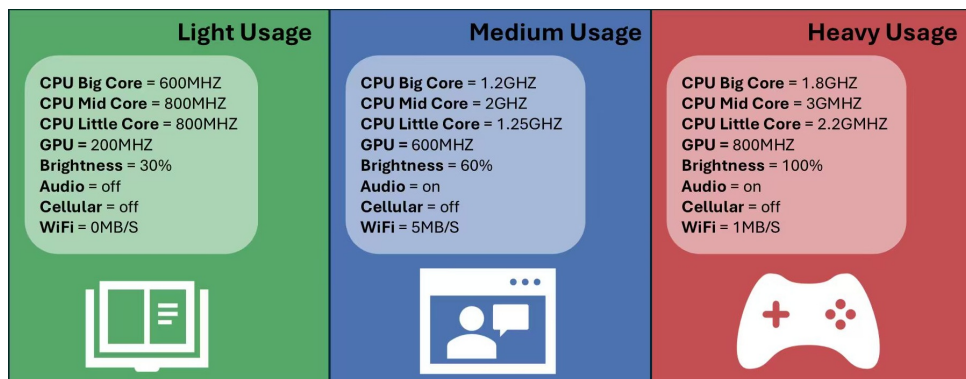


Figure 10: 3 scenarios

In this section, we focus on predicting the *Time-to-Empty* (TTE) of mobile devices. Based on the comprehensive power consumption model established earlier, we design

several representative usage scenarios to analyze the evolution of the battery state over time. Specifically, we assume that the device starts with a battery level of 100%, 75%, 50%, and 25%, and we compute the state of charge (SOC) as a function of time under light, medium, and heavy usage intensities. In addition, we simulate a typical user's mobile phone usage throughout a day to generate the SOC profile over time under realistic conditions.

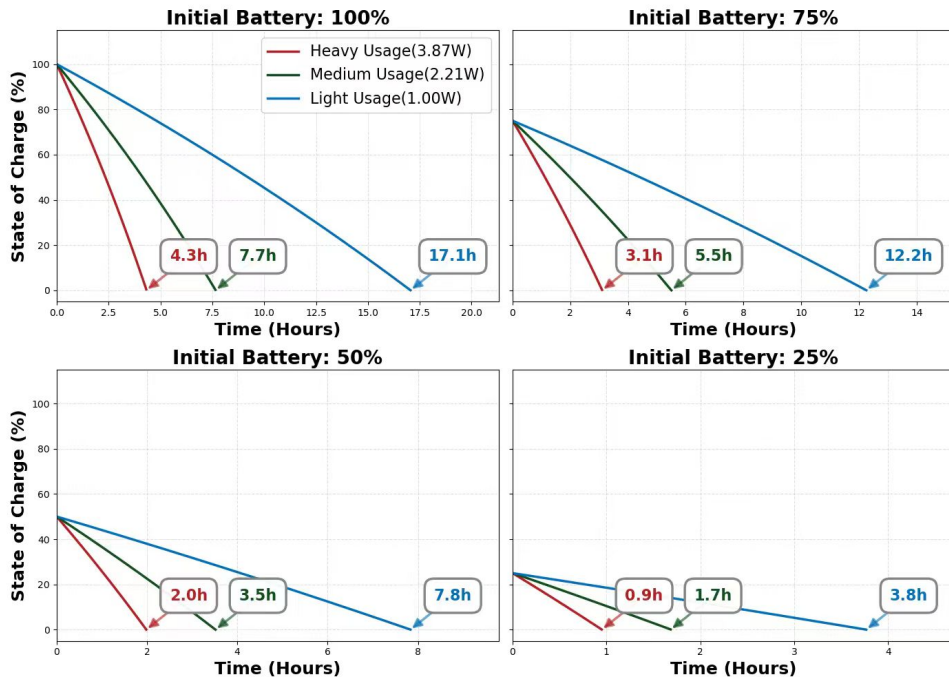


Figure 11: SOC Discharge Profiles by Initial Battery Level

In Figure 11, under the same initial state of charge, the battery depletes most rapidly under high-intensity usage, while light usage significantly extends the time-to-empty (TTE). For example, starting from a full charge, the TTE values are 17.1 hours (low), 7.7 hours (medium), and 4.3 hours (high). Moreover, heavy usage SOC leads to longer runtime, but the relationship between TTE and initial SOC is not strictly linear—lower SOC levels yield slightly less runtime per unit of charge, reflecting the nonlinear coupling between constant-power loading and voltage drop in the model. All SOC curves exhibit approximately linear decay over time, which validates the Coulomb-counting approach under the constant-power assumption.

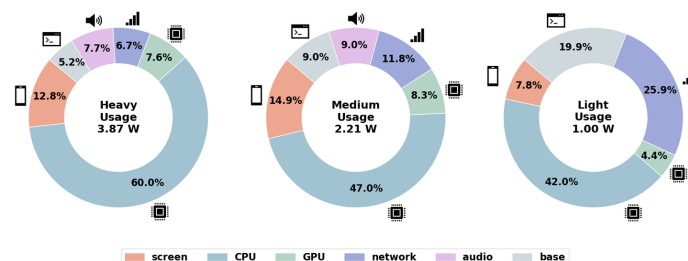


Figure 12: Power Consumption Breakdown

The Figure 12 illustrates the power consumption breakdown of a smartphone under high (3.87 W), medium (2.21 W), and low (1.00 W) usage intensities. Under high intensity (e.g., gaming), the CPU dominates at 60.0%. At medium intensity (e.g., video playback), the CPU accounts for 47.0%, with significant contributions from the display (14.9%) and network. Under low intensity (e.g., reading messages or attending class), the display becomes the largest consumer at 42.0%, while base power consumption rises to nearly 20%. These results highlight that **the CPU drives energy use under heavy load, whereas the display dominates under light load**, underscoring the need for context-aware power optimization strategies.

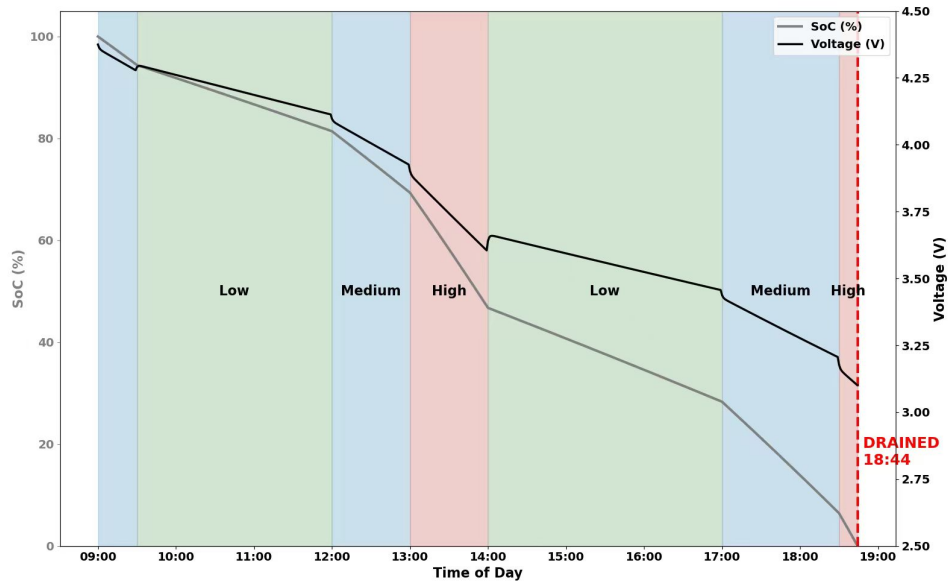


Figure 13: Full day electricity consumption simulation

The Figure 13 simulates a typical user's daily usage from 9:00 AM (starting at full charge) until battery depletion at 18:44, illustrating real-world battery runtime characteristics through the evolution of state of charge (SoC) and terminal voltage. Usage intensity is categorized into three levels: *light* (e.g., attending class, checking lecture slides), *medium* (watching videos), and *heavy* (gaming). During low-intensity periods (e.g., 9:00-12:00 and 14:00-17:00), the SoC declines gradually; it drops faster during medium-intensity video playback (12:00-13:00 and 17:00-18:00); and experiences a sharp decline in both SoC and voltage during the one-hour high-intensity gaming session (13:00-14:00), highlighting the disproportionate impact of peak loads on battery life. Although high-intensity usage accounts for only about 10% of total time, its energy consumption far exceeds that of other modes. The terminal voltage drops rapidly under heavy load, reflecting the transient effects of internal resistance and polarization. These results demonstrate that short-duration, high-power activities are the primary factor limiting battery runtime.

## 7 Sensitivity Analysis

To quantitatively assess the impact of key parameters on battery runtime, this study employs the *sensitivity factor*—defined as the ratio of the relative change in runtime to the relative change in a given parameter—to evaluate ambient temperature,

cycle count (representing battery aging), and baseline power consumption. The sensitivity factor is expressed as

$$S = \frac{\Delta Y/Y_0}{\Delta X/X_0}, \quad (27)$$

where  $Y$  denotes runtime and  $X$  the input parameter. A higher  $S$  indicates greater model sensitivity to parameter uncertainty. The factors are analyzed below in descending order of sensitivity.

## 7.1 Temperature and Cycle Count

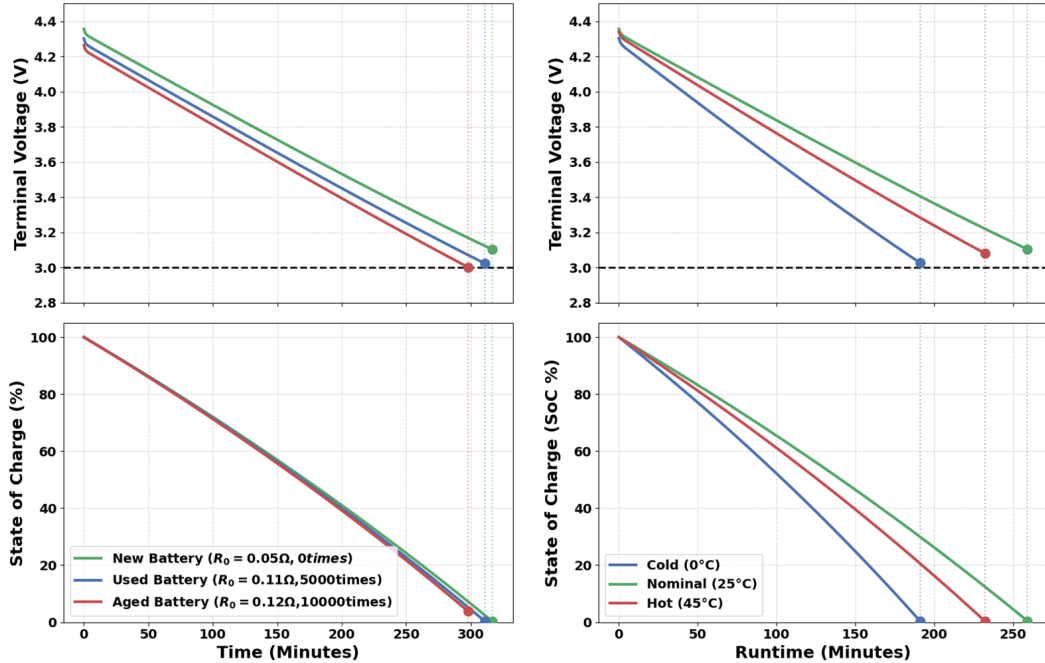


Figure 14: Sensitivity Analysis for Temperature and Cycle Count

In Figure 14, ambient temperature exhibits the highest sensitivity factor and represents the most critical external disturbance. Using 25 °C (298 K) as the baseline, a drop to 0 °C (273 K) reduces runtime from 250 min to 190 min—a 24% decline. The relative temperature change in absolute scale is approximately  $\Delta T/T_0 \approx 8.4\%$ , yielding a sensitivity factor of  $S_T \approx 2.86$ . This high sensitivity arises because low temperatures significantly increase internal resistance and suppress ion diffusion kinetics, causing premature voltage cutoff despite remaining capacity. As an uncontrollable environmental variable in real-world applications (e.g., electric vehicles or outdoor devices), temperature poses the greatest challenge to model robustness.

Cycle count—used to quantify battery aging—shows a moderate sensitivity factor, reflecting gradual but irreversible degradation. Relative to a fresh cell (0 cycles), a fully aged cell (10,000 cycles) sees runtime decrease from 320 min to 300 min (6.25% reduction). Treating the aging progression as a 100% relative change, the sensitivity factor is  $S_N \approx 0.0625$ . Although numerically small, this effect is physically significant: internal resistance  $R_0$  increases from 0.05 Ω to 0.12 Ω (+140%), accelerating voltage drop and triggering the 3.0 V cutoff earlier. Since aging is cumulative and cannot be mitigated during operation, it constitutes a medium-sensitivity factor in long-term deployment scenarios.

## 7.2 Baseline Power Consumption

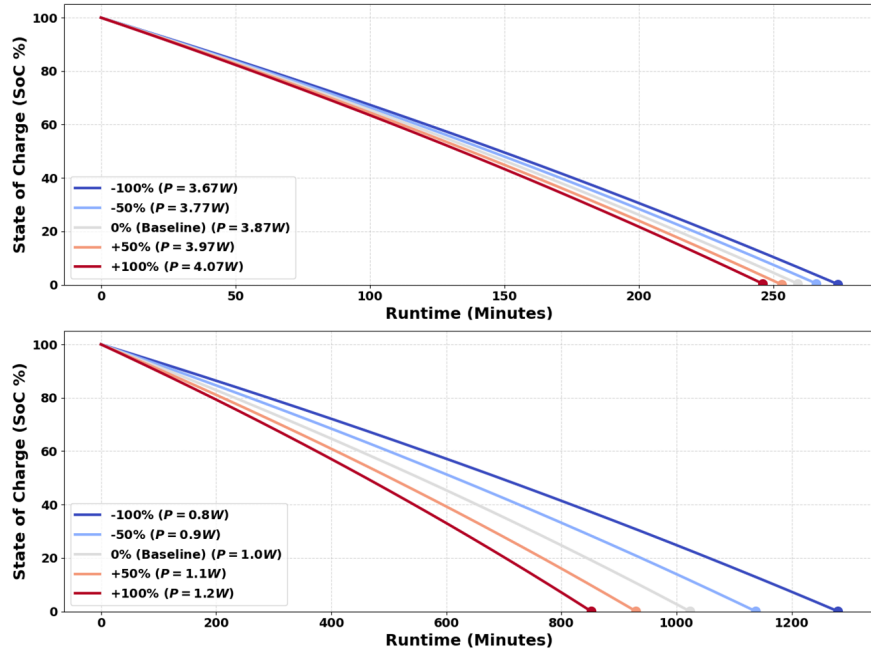


Figure 15: Sensitivity Analysis for Baseline Power Consumption

In Figure 15, baseline power consumption demonstrates the lowest sensitivity factor, despite causing large absolute changes in runtime. In a heavy-load scenario (nominal 3.87 W), a  $\pm 0.2$  W perturbation ( $\pm 5.2\%$ ) alters runtime by  $\pm 15$  min ( $\pm 5.8\%$ ), giving  $S_P \approx 1.12$ . In a low-power case (nominal 1.0 W), the same  $\pm 0.2$  W change ( $\pm 20\%$ ) leads to a 35% runtime variation, yielding  $S_P \approx 1.75$ . However, power draw maps linearly to discharge current ( $I = P/V$ ) and is typically well-controlled through system design (e.g., sleep modes, dynamic voltage scaling). Consequently, while power affects runtime substantially, its predictability and controllability render it the least threatening to model robustness under parameter uncertainty.

In summary, based on sensitivity factor analysis and physical interpretability, the ranking of influence on battery runtime is: **ambient temperature > cycle count > baseline power consumption**. This underscores that enhancing model adaptability to thermal variations and aging dynamics—not merely optimizing power usage—is essential for achieving robust battery performance prediction in real-world environments.

## 8 Recommendations

### 8.1 For Users

**Operate the device preferentially within a temperature range of 15°C-30°C and avoid prolonged use under extreme temperatures.**

Taking 25°C as the reference condition, when the ambient temperature decreases to 0°C, the effective battery life is reduced from approximately 250 minutes to 190 minutes, representing a decline of nearly 24%. The relative temperature change itself is only about 8.4%:

This disproportionate reduction indicates that low-temperature environments substantially accelerate battery depletion. Users are therefore advised to limit continuous usage in cold conditions or keep the device in an environment close to body temperature before operation.

**For aging devices, avoid high-load operations during low battery states.**

As battery aging progresses, the internal resistance increases from approximately  $0.05 \Omega$  to  $0.12 \Omega$ , corresponding to an increase of about 140%:

This rise significantly accelerates voltage drop during the later stages of discharge. Consequently, devices with aged batteries become markedly more sensitive to load variations at low state-of-charge levels. Users should complete computationally intensive tasks while sufficient battery capacity remains, rather than during low-battery operation.

**Short-term power fluctuations are tolerable, but sustained high-power usage should be avoided.**

Under moderate-to-high load conditions (approximately 3.87 W), a power variation of  $\pm 0.2 \text{ W}$  ( $\pm 5.2\%$ ) results in only about 15 minutes ( $\approx 5.8\%$ ) change in total battery life. This indicates that short-term power fluctuations have limited impact on user experience. However, sustained high-power usage leads to cumulative effects, which are particularly pronounced under non-ideal temperature conditions and may trigger premature shutdown.

## 8.2 For Manufacturers

**Treat ambient temperature as a primary control variable in battery management systems.**

Temperature variations exert a significantly greater influence on battery endurance than either power consumption or aging effects. A temperature change from 25°C to 0°C results in an approximate 24% reduction in battery lifefar exceeding the impact of comparable perturbations in other parameters. Therefore, energy management strategies should be automatically tightened when operating outside the 15°C–30°C range, rather than relying solely on remaining battery capacity as the control criterion.

**Address battery aging as a lifecycle constraint rather than an operational variable.**

As battery usage accumulates, internal resistance increases from  $0.05 \Omega$  to  $0.12 \Omega$ , causing the terminal voltage to reach the cutoff threshold earlier. Nevertheless, even under fully aged conditions, total battery life decreases only from approximately 320 minutes to 300 minutes (about 6.25%):

This indicates that aging effects are more appropriately handled through long-term design considerations and health assessment mechanisms, rather than frequent runtime interventions, which yield limited practical benefits.

**Focus power optimization on predictable and controllable system components.**

Under moderate load conditions, battery life exhibits substantially lower sensitivity to power fluctuations than to temperature variations. Moreover, the linear relation-

ship between power consumption and discharge current enables effective regulation through system-level design. Manufacturers are therefore advised to prioritize optimizations in controllable modules such as sleep-state management, voltage regulation, and background task scheduling rather than relying heavily on complex user behavior prediction.

### 8.3 Model Promotion

Originally developed for smartphones, this battery model has a story that reaches far beyond mobile devices. At its core is a simple yet physically grounded structure that links dynamic power loads to electrochemical battery response. This idea is broadly applicable. With minor modificationssuch as replacing the CPU and display with an electric motor and climate control system, and scaling capacity and internal resistance accordinglythe same framework can model electric vehicle batteries. The underlying equations governing state of charge and voltage dynamics remain valid. Whether powering a smartphone or an electric car, the physics of current, voltage, and energy depletion follow the same principles, and our model operates accurately across these diverse contexts.

## 9 Model Evaluation

### Strengths:

- **Physical interpretability:** The model explicitly captures the dynamics of SOC, polarization voltage, and instantaneous current, making its predictions physically meaningful.
- **Subsystem decomposition:** Total power consumption is broken down into major components including the screen, CPU, Wi-Fi, GPS, and cellular network, allowing detailed analysis of each subsystem's contribution.
- **External factor corrections:** Temperature, aging, and internal resistance variations are incorporated, significantly improving prediction accuracy under realistic operating conditions.
- **Robustness across operating conditions:** The model can handle different load profiles and usage scenarios, providing a practical framework for system-level energy analysis and optimization.

### Limitations:

- **Device-specific parameters:** Model parameters are derived from measurements on specific smartphones, which may limit generalizability to other devices.
- **Semi-empirical external corrections:** The internal resistance and external factor correction terms are based on semi-empirical formulas, which may introduce errors under rapidly changing or transient conditions.
- **Short-term high-frequency load variations:** Rapid fluctuations in power demand may not be fully captured.

- **Minor components not included:** Small energy-consuming modules, such as vibration motors or some sensors, are not explicitly modeled.

## 10 Conclusion

This paper addresses the practical challenge of smartphone battery runtime prediction by developing a mathematical model that integrates electrochemical principles with multi-factor power consumption analysis. Motivated by the gap between idealized battery models and the complexity of real-world usage, the proposed framework bridges fundamental electrochemical dynamics with contextual operational factors. Built upon a classical equivalent circuit structure, it effectively captures the dynamic evolution of the battery state of charge while systematically accounting for hardware workload, ambient temperature, and long-term aging effects.

The modular architecture of the model plays a central role in its effectiveness. By separating the core electrochemical representation from external usage modules, the approach preserves physical interpretability without sacrificing adaptability. This design enables seamless integration of diverse usage patterns and environmental conditions, making the model suitable not only for retrospective analysis but also for forward-looking battery management strategies. Further examination of factor interactions confirms that external conditions and cumulative degradation consistently dominate over transient power demands in shaping overall battery performance. These findings inform actionable guidance: users can adopt more battery-conscious behaviors, while manufacturers may enhance system-level designs through proactive thermal regulation and health-aware charging protocols.



Figure 16: Electric car battery photos(<https://www.autoexpress.co.uk>)

Beyond smartphones, the methodology exemplifies a general strategy for modeling energy systems where physical laws intersect with human behavior and environmental variability. By harmonizing mechanistic rigor with practical relevance, this work contributes not only a robust tool for mobile energy estimation but also a transferable framework for intelligent, interpretable modeling across a range of emerging energy-constrained technologies.

## References

- [1] XIONG W, WANG Y, HE Y, et al. State of charge estimation for lithium-ion batteries using model-based and data-driven methods: A review[J]. *IEEE Transactions on Vehicular Technology*, 2023, 72(6): 70937118.
- [2] ZHANG L, TIWANA B, QIAN Z, et al. Accurate online power estimation and automatic battery behavior based power model generation for smartphones[C]//*Proceedings of the Eighth IEEE/ACM/IFIP International Conference on Hardware/Software Codesign and System Synthesis*. New York: ACM, 2010: 105114.
- [3] DONG M, ZHONG L. Chameleon: A color-adaptive web browser for mobile OLED displays[C]//*Proceedings of the 9th International Conference on Mobile Systems, Applications, and Services*. New York: ACM, 2011: 8598.
- [4] SNOWDON D C, RUOCCHI S, HEISER G. Power management and dynamic voltage scaling: Myths and facts[C]//*Proceedings of the 2005 Workshop on Power Aware Real-time Computing*. New Jersey, USA, 2005: 3134.
- [5] VERMEER W, MOULI G R C, BAUER P. A comprehensive review on the characteristics and modeling of lithium-ion battery aging[J]. *IEEE Transactions on Transportation Electrification*, 2021, 8(2): 22052232.
- [6] ZHU Q, YU X, WU Q, et al. Semi-empirical degradation model of lithium-ion battery with high energy density[J]. *Energy Storage Science and Technology*, 2022, 11(7): 23242334.
- [7] GUÉGAIN É, RAES R, CHACHIGNOT N, et al. AndroWatts: Unpacking the power consumption of mobile devices components[C]//*2025 IEEE/ACM 12th International Conference on Mobile Software Engineering and Systems (MOBILESoft)*. Ottawa, ON, Canada: IEEE, 2025: 7181.
- [8] PRAMANIK P K D, SINHABABU N, MUKHERJEE B, et al. Power consumption analysis, measurement, management, and issues: A state-of-the-art review of smartphone battery and energy usage[J]. *IEEE Access*, 2019, 7: 182113182172.

## 11 Report on Use of AI Tools

### 1. Google Gemini(Jan 30, 2026 vision)

Query:"For this MCM Problem A, what key words can you provide with me and help me search for the articles?"

Output:"Lithium-ion battery equivalent circuit model (ECM), State of Charge (SOC) estimation differential equations, Lithium-ion battery equivalent circuit model (ECM)."

### 2. OpenAI ChatGPT(Feb 2, 2026 vision)

Upload the entire paper written in Mandarin to be translated into English.

### 3. Google Gemini(Feb 1, 2026 vision)

Auto-completions for code used in preparing our models, specifically for data cleaning and visualization scripts.

### 4. OpenAI ChatGPT(Feb 2, 2026 vision)

Query:"Based on our existing article, write a conclusion for about 200-300words"

Output:"This paper addresses the practical challenge of smartphone battery runtime prediction by developing a mathematical model that integrates electrochemical principles with multi-factor power consumption analysis. Motivated by the gap between idealized battery models and the complexity of real-world usage, the proposed framework bridges fundamental electrochemical dynamics with contextual operational factors. Built upon a classical equivalent circuit structure, it effectively captures the dynamic evolution of the battery state of charge while systematically accounting for hardware workload, ambient temperature, and long-term aging effects. The modular architecture of the model plays a central role in its effectiveness. By separating the core electrochemical representation from external usage modules, the approach preserves physical interpretability without sacrificing adaptability. This design enables seamless integration of diverse usage patterns and environmental conditions, making the model suitable not only for retrospective analysis but also for forward-looking battery management strategies. Further examination of factor interactions confirms that external conditions and cumulative degradation consistently dominate over transient power demands in shaping overall battery performance. These findings inform actionable guidance: users can adopt more battery-conscious behaviors, while manufacturers may enhance system-level designs through proactive thermal regulation and health-aware charging protocols."